Finite Element Analysis of Unnotched Charpy Impact Tests

D.Y. Jeong[1], H. Yu[2], J.E. Gordon[1], Y.H. Tang[1]
[1] U.S. Department of Transportation, Volpe National Transportation Systems Center, Cambridge, Massachusetts, USA
[2] Chenga Advanced Solutions & Engineering LLC, Cambridge, Massachusetts, USA

Keywords: Charpy energy, finite element analysis, fracture, material failure, stress triaxiality

Abstract

This paper describes nonlinear finite element analysis (FEA) to examine the energy to fracture unnotched Charpy specimens under pendulum impact loading. An oversized, nonstandard pendulum impactor, called the Bulk Fracture Charpy Machine (BFCM), was constructed to conduct studies to assess the fracture behavior of various tank car steels. Comparisons between measured and calculated impact energies are presented. The effect of various factors on impact energy is demonstrated through the test data and FEA results. These factors include striker size and shape, specimen thickness, and specimen material. Moreover, calculations of fracture energy are carried out using FEA in conjunction with different material failure criteria. The FEA results using a failure initiation criterion based on the general state of stress in terms of stress triaxiality and a failure progression model based on linear strain softening are shown to provide excellent agreement with the experimental data.

Introduction

Accidents involving the transport of hazardous materials by railroad tank cars are rare occurrences, but their consequences can be severe. A review of accident data since the mid-1960s indicates that release of toxic inhalation hazard materials from accident events such as train-to-train collisions and derailments are usually caused by failures in three general locations in tank cars: (1) tank end or head (2) tank car side or shell, and (3) valves and fittings [1].

The Volpe National Transportation Systems Center provides technical support to the Federal Railroad Administration (FRA) by conducting and managing research to examine the structural integrity and crashworthiness of railroad tank cars carrying hazardous materials. Moreover, the objective of FRA-sponsored research is to maintain tank integrity under a broad range of conditions that vary from the normal operating environment to rare but extreme circumstances such as impact loads during accidents. During the course of this research, scaled and full-scaled impact tests have been conducted to examine the puncture resistance of railroad tank cars [2], but the mechanics of material failure under dynamic impact loading are not well understood. Moreover, no industry-accepted standard exists to quantify the puncture behavior of materials used to construct railroad tank cars.

Previous research to examine the resistance of tank car steels to impact loading has focused on fracture toughness or Charpy V-Notch (CVN) energy. Industry-accepted procedures have been developed to conduct these tests, which use specimens containing a pre-existing crack (usually fatigue-sharpened) or a stress concentration or notch. However, the physical

significance of fracture toughness or CVN impact energy in a structure without a pre-existing crack is unclear.

Pendulum impact testing, such as the standard CVN test, has been used to examine the impact resistance of materials for over a century because it is relatively simple, inexpensive, and rapid to perform [3]. In addition, the physical interpretation of the test is clear. The energy available to fracture the specimen is proportional to the initial height of the swing hammer above a reference level (y_1 in Figure 1). The energy remaining in the hammer is characterized by the height to which it recovers (y_2), and the weight of the striker times the difference (y_1–y_2) represents the energy absorbed by the specimen. The physics of the pendulum impact test are the same whether the specimen contains a notch or not. However, more energy is needed to fracture an unnotched specimen than one containing a pre-existing notch.

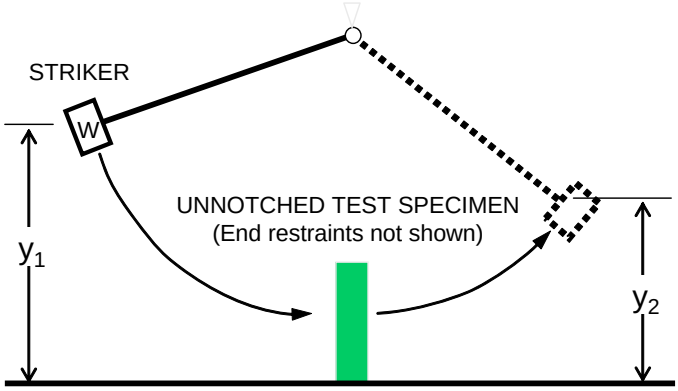

Figure 1 Schematic of pendulum impact test

An oversized, nonstandard pendulum impactor was built by Southwest Research Institute (SwRI) to examine the fracture energy of different tank car steels. Figure 2 shows photographs of this pendulum test fixture, which is called the Bulk Fracture Charpy Machine (BFCM). The size of the fixture was necessary to achieve the levels of energy needed to fracture the unnotched specimens. Moreover, the BFCM was constructed specifically to conduct studies to assess puncture behavior. That is, the measurement of fracture energy is used to assess the puncture resistance of tank car steel.

Figure 3 shows a detailed drawing of the BFCM test specimen. The trapezoidal ends of the specimen self-engage into the test fixture, so they are held fixed as the impact load is applied through the pendulum. In this drawing, the test section is 15.24 cm (6 inches) long, and the specimen width is 2.54 cm (1 inch). Specimen thickness ranged between 4.83 and 21.1 mm (0.19 and 0.83 inch).

Figure 4 shows detailed drawings of the two impact tups or strikers that were used in the BFCM tests. The blunt tup has a contact surface width of 12.7 mm (0.5 inch) with a 2.54-cm (1-inch) radius; the sharp tup has a contact surface width and radius of 3.18 mm (0.125 inch).

Figure 2 Bulk Fracture Charpy Machine (BFCM) for pendulum impact testing

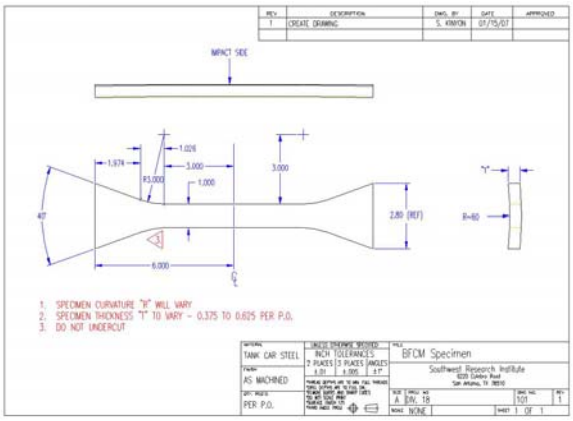

Figure 3 BFCM test specimen

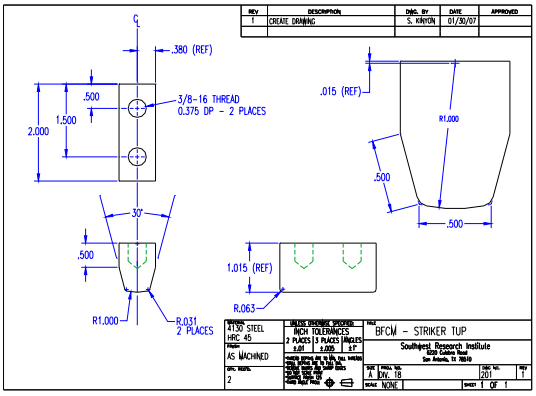

(a) Blunt tup

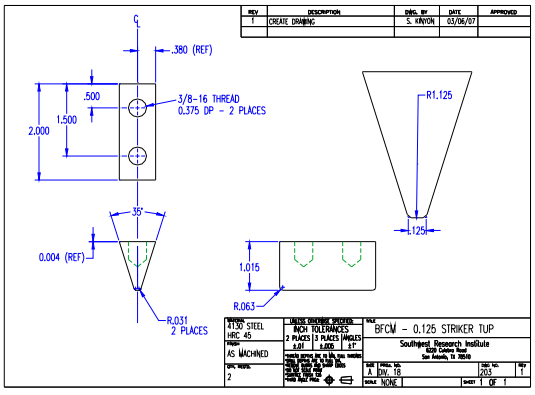

(b) Sharp tup

Figure 4 Impact tups used in BFCM tests

Finite Element Model with Damage Initiation and Progression to Failure

The FEA models developed to examine the energy to fracture unnotched Charpy specimens account for the following physical aspects of the problem at hand: (1) elastic-plastic material behavior, and (2) initiation and progression of damage leading to material failure. These models were developed using the commercial finite element code ABAQUS/Explicit [5], which includes standard elastic-plastic constitutive material models and a resident damage initiation and evolution model based on stress triaxiality and strain softening.

Three-dimensional solid elements are used to generate the finite element mesh at and around the region of impact. Moreover, a patch of three-dimension solid or brick elements with aspect ratio equal to one and a minimum of six elements through the thickness are meshed in the vicinity of the impact zone. This patch can be coupled to shell elements at locations away from the impact location that do not require this special treatment. Shell elements in the impact zone are inadequate to produce accurate results in simulating the initiation and progression of damage leading to material failure.

The failure criteria used in this paper assume that the onset of failure (i.e., failure initiation) occurs when loading conditions produce effective plastic strains that exceed a certain threshold. This threshold or critical strain is further assumed to depend on the general state of stress in terms of stress triaxiality.

Stress triaxiality describes the portion of the stress tensor that is hydrostatic. Mathematically, stress triaxiality is the ratio of mean stress to effective or von Mises equivalent stress, or

$$\eta = \frac{\sigma_m}{\sigma_e} \tag{1}$$

In terms of principle stresses, the mean stress and the effective or von Mises equivalent stress are defined respectively as

$$\sigma_m = \frac{1}{3}\left(\sigma_1 + \sigma_2 + \sigma_3\right) \tag{2}$$

$$\sigma_e = \sqrt{\frac{1}{2}\left[\left(\sigma_1 - \sigma_2\right)^2 + \left(\sigma_2 - \sigma_3\right)^2 + \left(\sigma_3 - \sigma_1\right)^2\right]} \tag{3}$$

Mean or hydrostatic stress is associated with dilatation or the change in volume of a solid element as it deforms. Effective or von Mises stress is directly related to octahedral shearing stress, which in turn is related to distortional energy or the energy to change the shape of a solid element as it deforms. Therefore, a physical interpretation of stress triaxiality is that it describes the general state of stress in a solid element and is related to the ratio of volume change to shape change.

The material failure criterion that is used primarily in this paper is attributed to Bao and Wierzbicki [6]. Figure 5 is a schematic of this criterion, which illustrates effective strain to initiate failure, $\bar{\varepsilon}_i^{pl}$ as a function of stress triaxiality, η. The Bao-Wierzbicki (B-W) failure initiation envelope is shown to consist of three regions representing different modes of failure.

Region I is related to high levels of stress triaxiality which promotes nucleation, growth, and coalescence of voids leading to ductile fracture. Region III is negative values of stress triaxiality which represent shear fracture due to shear band localization. Region II comprises positive but low levels of stress triaxiality representing mixed mode fracture. The schematic also shows that zero stress triaxiality is equal to a stress state of pure shear, and that the cusp between Regions I and II is equal to a stress state of uniaxial tension.

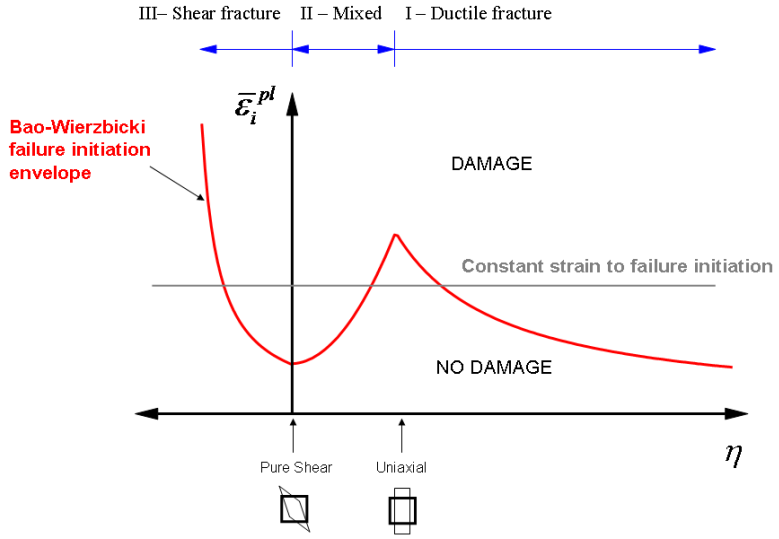

Figure 5 Schematic of failure initiation envelope based on stress triaxiality

Failure initiation occurs when loading conditions induce effective plastic strains at levels above the limits suggested by Figure 5. Once failure initiates, damage is assumed to progress in the form of linear strain softening. Figure 6 illustrates the concept, in which the stress-strain behavior of a material element exhibits a linear decrease in stress with increasing strain beyond the strain to initiate failure, ε_i. Modeling damage progression by strain softening helps minimize the mesh dependency of the numerical results [7].

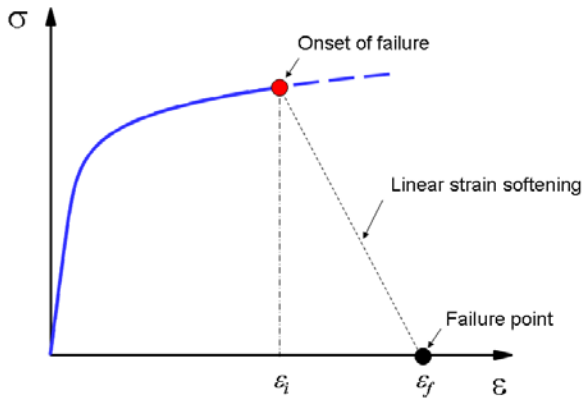

Figure 6 Schematic of linear strain softening

Other material failure criteria have been developed that depend on the general state of stress in terms of stress triaxiality [8]. The merit of the Bao-Wierzbicki criterion is that it accounts for various failure modes as shown schematically in Figure 5. Other criteria appear to be limited to a single mode of failure. For example, Gurson [9] and Tvergaard [10] developed a criterion to model ductile fracture, which considers only Region I of the Bao-Wierzbicki envelope. In addition, results are presented in this paper based on a constant strain criterion, which is shown schematically in Figure 5 for comparison. Clearly, constant strain may be a considered as a special case of the Bao-Wierzbicki failure envelope in which effective plastic strain to initiate failure is independent of stress triaxiality, but the level at which failure initiation is specified to occur is arbitrary.

In theory, the failure initiation envelope for a given material is developed through a series of physical tests. The complete series entails eleven tests with different specimen geometries to characterize different levels of near-constant stress triaxiality in the vicinity of failure. Such tests were conducted previously to develop failure initiation envelopes for 2024-T351 aluminum [11] and A710 steel [12]. In the present implementation, the failure initiation envelope for different tank cars steels is constructed from a calibration method using measurements from standard uniaxial tensile tests [13]. According to Lee and Wierzbicki [13], this calibration method estimates a failure initiation envelope that is within 10 percent agreement of that based on the complete tests series.

BFCM test specimens were made from four different steels, which include TC-128B, A710, HPS 70, and HPS 100. Two batches of normalized TC-12B tank car steel were used in the tests. Conventional railroad tank cars are built with normalized TC-128B steel. The other materials are considered as high strength-low alloy or high performance strength (HPS) steels, and are typically used in other applications (e.g., HPS 70 is used in the construction of bridge structures). Table 1 lists the mechanical properties for these steels as measured in the longitudinal orientation from standard uniaxial tensile tests.

Table 1 Measured uniaxial tensile properties for different steels

	Ultimate Tensile Strength		Yield Strength		Elongation	Reduction in Area
	(MPa)	(ksi)	(MPa)	(ksi)	(%)	(%)
TC-128B, Batch 1	602	87.3	408	59.2	27.0	58.0
TC-128B, Batch 2	630	91.3	447	64.8	28.0	59.0
A710	621	90.0	553	80.2	31.0	67.4
HPS 70	662	96.0	517	75.0	23.0	63.4
HPS 100	818	118.7	738	107.1	23.0	73.2

Failure initiation envelopes for different steels were constructed based on a modified version of the Lee and Wierzbicki calibration method [13]. The stress-strain relation is assumed to follow a power law:

$$\sigma = K\varepsilon^n \tag{4}$$

where σ and ε are stress and strain respectively. In addition, K and n are empirical constants that are determined from the properties listed in Table 1. Moreover, the Bao-Wierzbicki failure initiation envelope is approximated by the following functional form [13]:

$$\bar{\varepsilon}_i^{pl} = \begin{cases} \infty & \eta \le -1/3 \\ C_1 / (1+3\eta) & -1/3 < \eta \le 0 \\ C_1 + (C_2 - C_1)(\eta/\eta_o)^2 & 0 < \eta \le \eta_o \\ C_2 \eta_o / \eta & \eta_o < \eta \end{cases} \tag{5}$$

where $\bar{\varepsilon}_i^{pl}$ is the effective plastic strain to initiate failure, C_1 is equal to $\bar{\varepsilon}_i^{pl}$ in pure shear and C_2 is $\bar{\varepsilon}_i^{pl}$ in uniaxial tension. In addition, η_o is the value of stress triaxiality corresponding to uniaxial tension, and is assumed to be constant and equal to ⅓. The constants C_1 and C_2 are determined from the following equations

$$C_1 = C_2 \left(\frac{\sqrt{3}}{2} \right)^{1/n} \qquad C_2 = \ln\left(\frac{1}{1 - RA} \right) \tag{6}$$

where RA is the reduction in area. Table 2 lists the parameters for the failure criterion based upon application of these equations. In addition, Figure 7 shows the failure envelopes in terms of effective plastic strain to initiate failure as a function of stress triaxiality.

Table 2 Calibrated parameters for B-W failure criterion

	K		n	C_1	C_2
	(MPa)	(ksi)			
TC-128B, Batch 1	793	115.0	0.160	0.224	0.868
TC-128B, Batch 2	772	112.0	0.115	0.256	0.892
A710	719	104.3	0.049	0.060	1.121
HPS 70	815	118.2	0.084	0.182	1.005
HPS 100	947	137.3	0.048	0.065	1.317

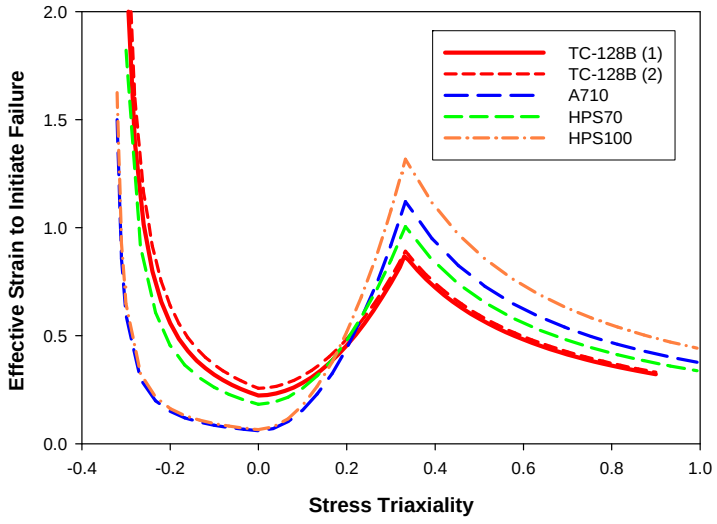

Figure 7 Bao-Wierzbicki failure initiation envelopes for different steels

Results

The FEA models were used to simulate the BFCM tests on specimens with varying thicknesses made from TC-128B tank car steel. The FEA models incorporated the Bao-Wierzbicki material failure criterion. Figure 8 shows FEA and experimental results for fracture energy as a function of specimen thickness for the blunt and sharp strikers. The error bars represent the variability in the test data in terms of two standard deviations above and below the average value for a given specimen thickness. The dashed lines represent best-fit regression curves to the averages of the data. The FEA results and the BFCM test data clearly show that more energy is required to fracture an unnotched Charpy specimen using the blunt tup than with the sharp tup. Moreover, the FEA results are within reasonable agreement with the test data.

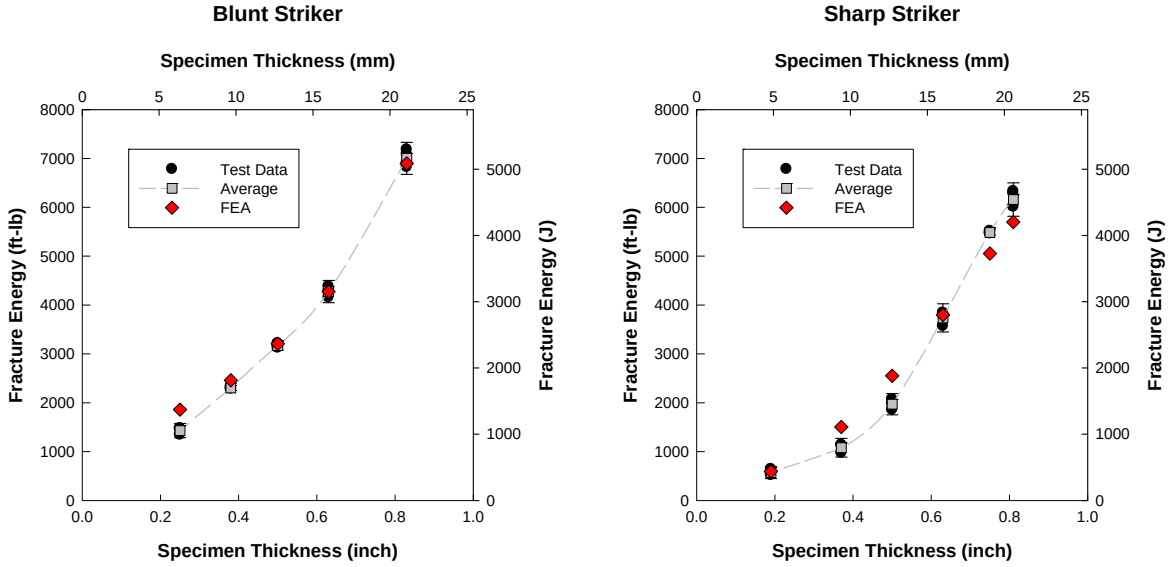

Figure 8 Measured and calculated fracture energy as a function of specimen thickness for TC-128B

Figure 9 shows the evolution of stress triaxiality during two BFCM tests, one using the blunt striker and the other using the sharp tup. The specimens in these two cases have comparable thickness; 21.1 mm (0.83 inch) for the blunt case and 20.6 mm (0.81 inch) for the sharp case. The two specific locations of interest are called out in Figure 10, which is a still from a BFCM test using the sharp striker. The two locations are referred to as (1) the impacted surface; i.e., the side on which the striker contacts the specimen, and (2) the free surface; i.e., the opposite or free side of the test specimen. Moreover, the plots shown in Figure 9 are referred to stress triaxiality maps since they show effective plastic strain to initiate failure as a function of stress triaxiality. The symbols in the plot correspond to different time steps for the two specific locations of interest. The Bao-Wierzbicki failure initiation envelope is overlayed, which is represented by the solid blue curve. The solid red circles represent the same instant in time, which corresponds to the onset of failure. The stress triaxiality map for the case using the blunt tup indicates that the onset of failure occurs on the free surface of the specimen or the side of the test specimen opposite to the impacted surface. In the case using the sharp tup, however, the onset of failure occurs at the impacted surface of the specimen. Damage then propagates through the specimen thickness in the direction that the striker penetrates material.

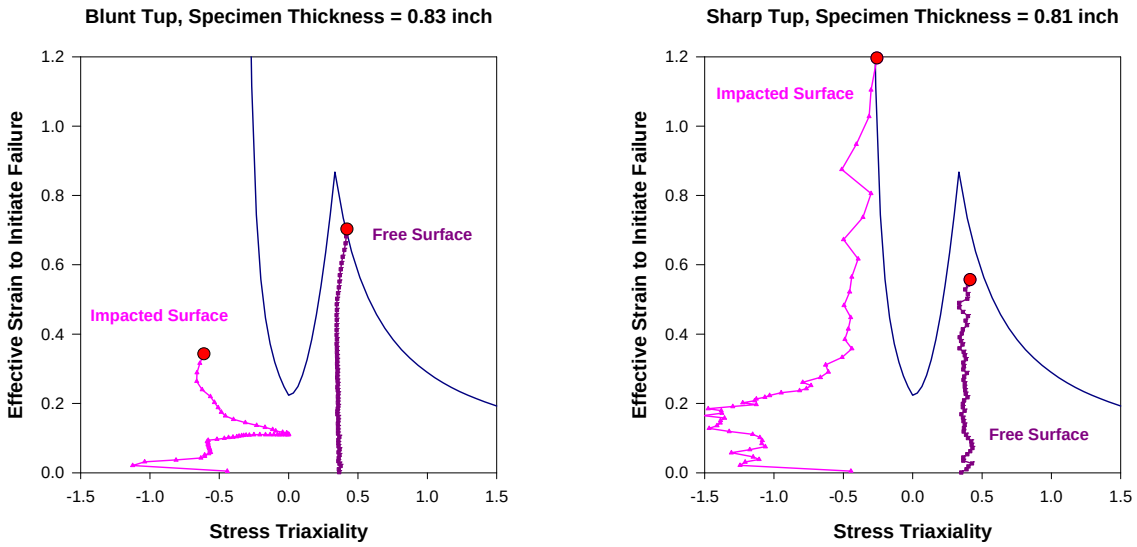

Figure 9 Stress triaxiality maps for BFCM tests

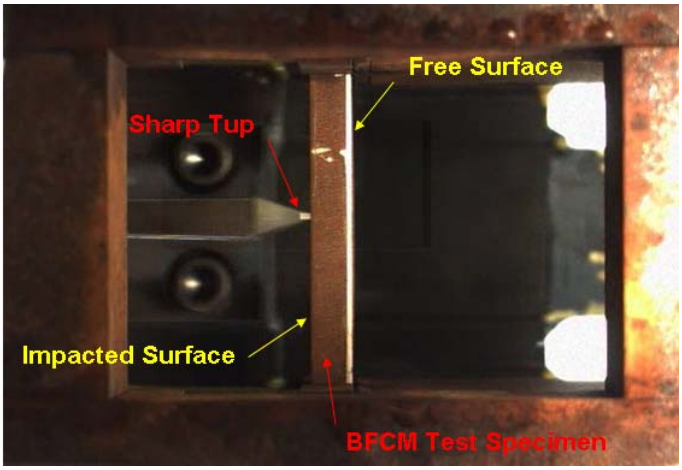

Figure 10 Still from BFCM test using sharp tup

The stress triaxiality maps show that the failure modes on the impacted and free surfaces of the BFCM specimen are different. Failure on the impacted surface is driven by the localization of shear stresses. Failure on the free surface occurs from ductile fracture. Moreover, stress triaxiality maps from FEA simulations on full-scale tank car shell impact tests resemble those of the BFCM tests using the blunt striker. That is, failure in the full-scale tank car tests appears to initiate on the inside surface of the tank [14].

Figure 11 compares FEA results with and without strain softening assumed with the BFCM test data for TC-128B steel using both the blunt and sharp strikers. The figure clearly shows that the FEA results without strain softening tend to underestimate the energy to fracture unnotched Charpy specimens. This is because a portion of the strain energy is neglected if strain softening is not taken into account. Moreover, these results indicate that strain softening has a significant effect on the calculated energy to fracture.

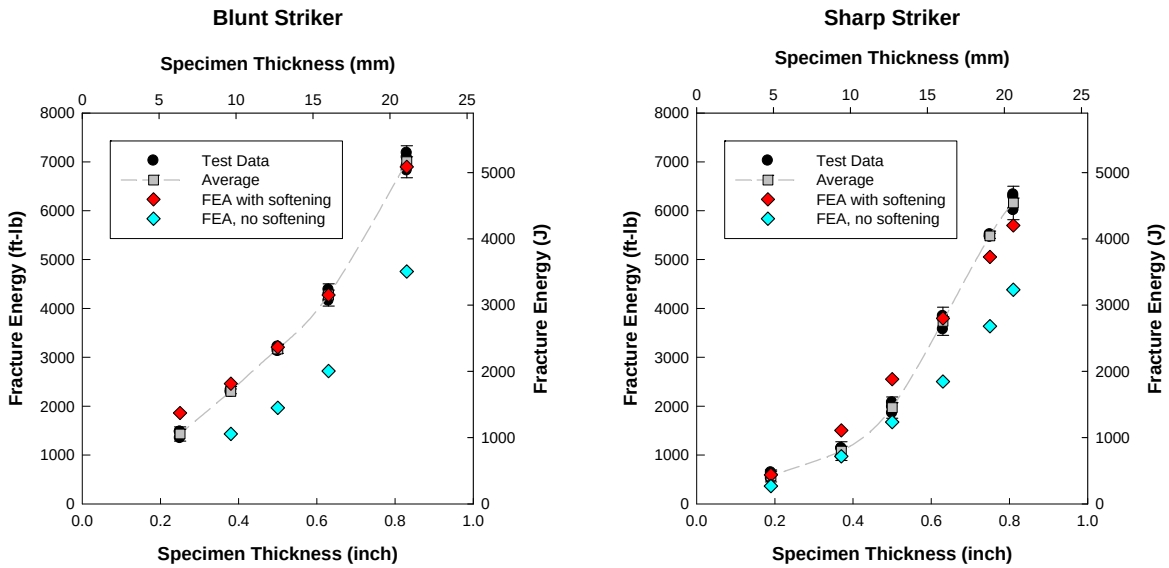

Figure 11 Effect of strain softening on calculated BFCM fracture energy (TC-128B)

Figure 12 compares FEA results using different material failure criteria to mimic the BFCM test data on TC-128B steel using the blunt striker. In the FEA results assuming constant strain, a critical value of 20 percent strain was assumed for the strain to initiate failure. FEA results assuming both criteria exhibit a nonlinear variation of fracture energy with specimen thickness. When the constant strain criterion is applied, the agreement between test and analysis is very good for the thinner specimens. When the B-W criterion is applied, the range of specimen thickness in which the FEA results accurately reproduce the test data corresponds to the range that is typically used in construction of railroad tank cars.

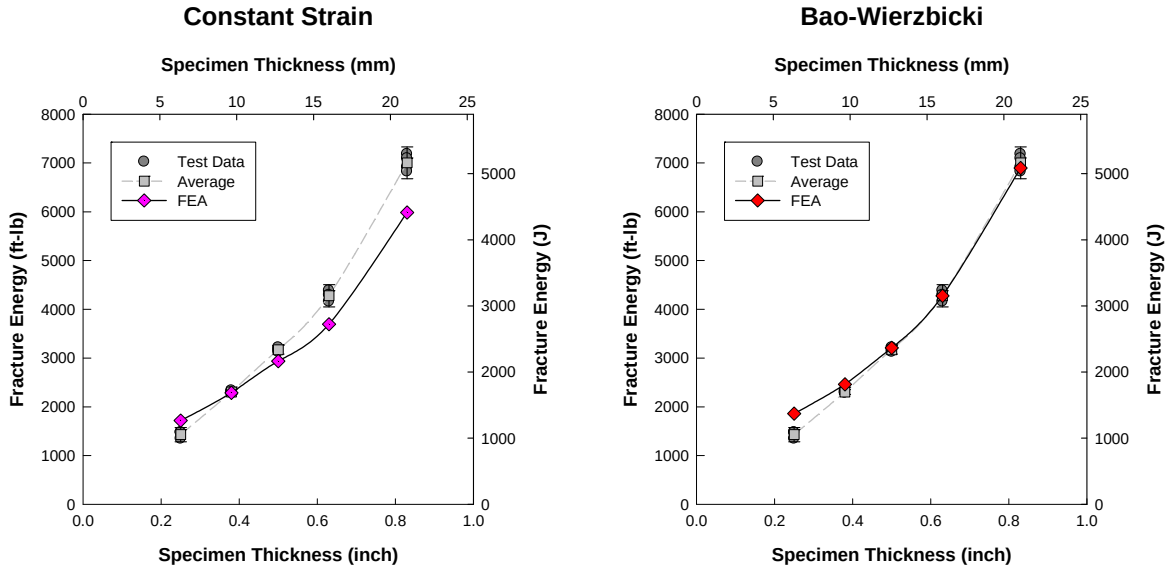

Figure 12 Comparison of different criteria for TC-128B (Blunt Striker)

FEA in conjunction with the Bao-Wierzbicki criterion was applied to simulate the BFCM tests using different steels. Figure 13 compares the measured and FEA calculated fracture energies for unnotched Charpy specimens made from different steels impacted by the blunt tup. The figure indicates that the agreement between the calculated and measured fracture energies is good.

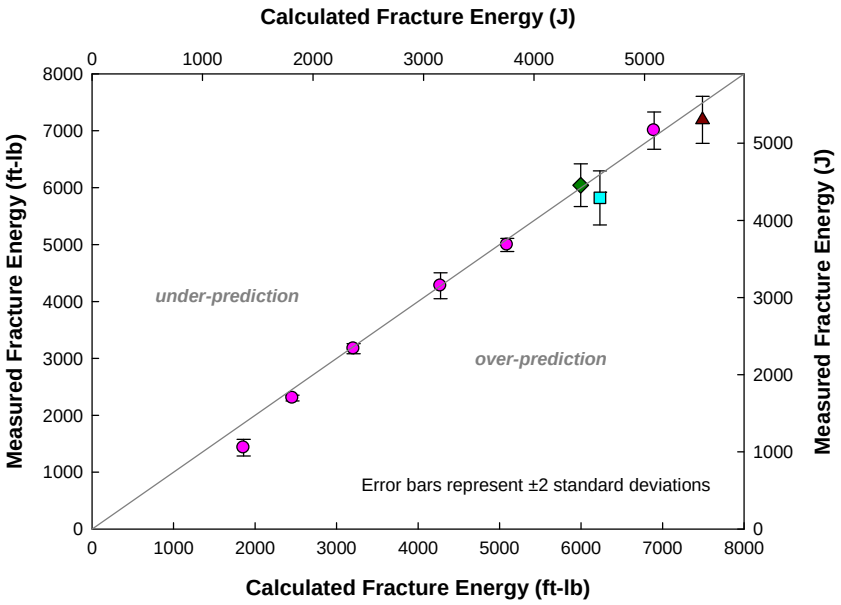

Figure 13 Comparison between measured and calculated fracture energies for different steels (Blunt Striker)

Concluding Remarks

Elastic-plastic finite element analysis (FEA) was conducted to simulate pendulum impact testing of unnotched Charpy specimens using a dedicated fixture called the Bulk Fracture Charpy Machine (BFCM). Simulation and experimental results were compared on the basis of the energy required to fracture the specimens under a variety of test conditions. Different impact strikers or tups were used in the BFCM. Specimen thickness was varied for the tests conducted on normalized TC-128B tank car steel. In addition, test specimens were made from different types of steel.

Elastic-plastic FEA used in conjunction with a material failure criterion based on stress triaxiality followed by linear strain softening produced results within the narrow scatter band of the test results for all specimen thicknesses greater than 12.7 mm (0.5 inch). The range of thickness in which the analysis most accurately reproduced the experimental data corresponds to that used in typical railroad tank car construction. This favorable outcome suggests that the FEA framework with the assumed failure criterion; namely, the Bao-Wierzbicki criterion, may be applied to other impact loading cases; such as tank car shell impacts [14].

Acknowledgments

The work described in this paper was sponsored by the Federal Railroad Administration, Office of Research and Development. Mr. Francisco Gonzalez is the FRA project manager for research on railroad tank cars. Mr. Eloy Martinez also provides technical direction to the project. Technical discussions with Professor A. Benjamin Perlman of the Volpe Center are greatly appreciated.

References

[1] Treichel, T., 2006: "List of Accident-Caused Releases of Toxic Inhalation Hazard (TIH) Materials from Tank Cars, 1965-2005," RSI-AAR Railroad Tank Car Safety Research and Test Project, Report No. RA 06-05.

[2] Phillips, E.A., Olsen, L., 1972: "Final Phase 05 Report on Tank Car Head Study," RPI-AAR Tank Car Safety Research and Test Project, RA-05-17.

[3] Siewert, T.A., Manahan, Sr., M.P., Eds. 2000: *Pendulum Impact Testing: A Century of Progress, STP 1380,* American Society for Testing and Materials, West Conshohocken, PA.

[4] McKeighan, P., 2007: "Mechanical Properties of Tank Car Steels Retired from the Fleet," Southwest Research Institute Report to the Volpe Center.

[5] ABAQUS Inc., 2006: ABAQUS Analysis User's Manual.

[6] Bao, Y., Wierzbicki, T., 2004: "On fracture locus in the equivalent strain and stress triaxiality space," *International Journal of Mechanical Sciences 46,* 81-98.

[7] Hillerborg, A., Modeer, M., Petersson, P.E., 1976: "Analysis of crack formation and crack growth in concrete by means of fracture mechanics and finite elements," *Cement and Concrete Research 6*, 773-782.

[8] Wierzbicki, T., Bao, Y., Lee, Y.W., Bai, Y., 2005: "Calibration and evaluation of seven fracture models," *International Journal of Mechanical Sciences 47,* 719-743.

[9] Gurson, A.L., 1977: "Continuum Theory of Ductile Rupture by Void Nucleation and Growth: Part 1 – Yield Criterion and Flow Rules for Porous Ductile Media," *Journal of Engineering Materials and Technology 99,* 2-15.

[10] Tvergaard, V.: 1981: "Influence of Voids on Shear Band Instabilities under Plane Strain Conditions," *International Journal of Fracture 17,* 389-407.

[11] Bao, Y., Wierzbicki, T., 2002: "Determination of Fracture Locus for the 2024-T351 Aluminum," Massachusetts Institute of Technology, Impact and Crashworthiness Laboratory Report No. 81.

[12] Bao, Y., Bai, Y., Wierzbicki, T., 2004: "Calibration of A710 Steel for Fracture," Massachusetts Institute of Technology, Impact and Crashworthiness Laboratory Report No. 135.

[13] Lee, Y.W., Wierzbicki, T., 2004: "Quick Fracture Calibration for Industrial Use," Massachusetts Institute of Technology, Impact & Crashworthiness Laboratory Report No. 115.

[14] Tang, Y.H., Yu, H., Gordon, J.E., Jeong, D.Y., Perlman, A.B., 2008: "Analysis of Railroad Tank Car Shell Impacts Using Finite Element Method," *Proceedings of the 2008 IEEE/ASME Joint Rail Conference*, JRC2008-63014.